Global and Planetary Change 204 (2021) 103557

Contents lists available at ScienceDirect

Global and Planetary Change

journal homepage: www.elsevier.com/locate/gloplacha

Influence of stationary waves on mid-Pliocene atmospheric rivers and hydroclimate

Sofia Menemenlis[a,*], Juan M. Lora[a], Marcus Lofverstrom[b], Deepak Chandan[c]

[a] Dept. of Earth and Planetary Sciences, Yale University, 210 Whitney Ave, New Haven, CT 06511, USA
[b] Dept. of Geosciences, University of Arizona, 1040 E 4th St, Tucson, AZ 85719, USA
[c] Dept. of Physics, University of Toronto, 60 St. George Street, Toronto, ON M5S1A7, Canada

ARTICLE INFO

Keywords:
Pliocene
Atmospheric rivers
Extreme precipitation
Stationary waves

ABSTRACT

The mid-Pliocene warm period (~3.3–3 million years ago) sustained similar atmospheric CO_2 concentrations to today, and is thus considered one of the best recent paleoclimate analogs for a future warmer climate. Using model simulations following the Pliocene Model Intercomparison Project Phase 2 experimental design, we investigate the mid-Pliocene mid-latitude hydroclimate with a focus on Pacific atmospheric rivers and related changes to mean and extreme precipitation over the Americas. We find distinct spatial patterns of change in precipitation compared to the pre-industrial control simulation in the northern and southern hemispheres; specifically, the Pacific coasts of North America and Chile, two regions where atmospheric rivers strongly influence local weather and climate today, experience opposite signs of change in precipitation. The precipitation changes are linked to dynamical shifts in atmospheric rivers, especially in the Northern Hemisphere. There, a wintertime stationary wave train present in the pre-industrial control nearly disappears in the mid-Pliocene simulation, resulting in fewer atmospheric rivers making landfall over western North America. Sensitivity simulations reveal that model boundary conditions for mid-Pliocene ice sheets and topography, applied in isolation or in combination, cause the relevant stationary wave response independently of CO_2 forcing. The stationary wave response to surface boundary conditions weakens the analogy between mid-Pliocene and future regional midlatitude hydroclimate, and informs our interpretation of the apparent discrepancy between modeled precipitation and hydroclimate proxies in western North America.

1. Introduction

The Pliocene epoch, during which global temperatures exceeded those of the present, offers an opportunity to study the Earth system response to warming on time-scales longer than those accessible through observational records. While the more recent Pleistocene interglacials were warmer than the pre-industrial, these intervals were ephemeral; the Pliocene represents the most recent sustained period of elevated warmth. For the past three decades, research efforts combining numerical modeling and proxy data have furthered our understanding of the Pliocene, with a particular focus on the mid-Pliocene warm period ~3.3–3 million years ago (Ma) (Haywood et al., 2016a, 2020).

Mid-Pliocene atmospheric CO_2 levels (pCO_2) are estimated to have fallen between 350 and 450 ppm by volume (ppmv), a range encompassing present-day concentrations (Pagani et al., 2010; Bartoli et al., 2011; Badger et al., 2013; Martínez-Botí et al., 2015). Because Earth's physical characteristics—including its topograpy, bathymetry, and continental configuration—were generally similar to the present (Dowsett et al., 2016; Haywood et al., 2016a), the mid-Pliocene serves as a useful test-case for studying processes relevant to future climate change. Understanding this period in Earth's history may reveal longer-term (i.e., equilibrium) impacts and feedbacks of CO_2-induced warming that are difficult to ascertain from comparatively short, transient simulations of future climate change (Kageyama et al., 2018).

The Pliocene Model Intercomparison Project phase 2 (PlioMIP2) is an international collaboration to quantify uncertainties in and improve upon model simulations of the warm Pliocene climate (Haywood et al., 2016b). Results indicate that Earth-system sensitivity (ESS), which is the Earth's temperature response to a doubling of pCO_2 after incorporating slow feedback processes such as changes in ice sheets and vegetation, exceeded equilibrium climate sensitivity (ECS), which does not include these slow feedbacks, by approximately 50% (Haywood et al., 2020).

* Corresponding author.
E-mail address: sofia.menemenlis@yale.edu (S. Menemenlis).

https://doi.org/10.1016/j.gloplacha.2021.103557
Received 11 December 2020; Received in revised form 7 May 2021; Accepted 28 June 2021
Available online 3 July 2021

Warming was enhanced in high-latitude regions ("polar amplification") and meridional sea surface temperature gradients were reduced, though most PlioMIP2 models still underestimate high latitude surface air temperatures compared to proxy reconstructions (McClymont et al., 2020; de Nooijer et al., 2020; Haywood et al., 2020). Some proxy and modeling studies have argued for substantially reduced zonal temperature gradients in the tropics during various sub-intervals of the Pliocene (Wara et al., 2005; Christina Ravelo et al., 2006; Burls and Fedorov, 2014; Fedorov et al., 2015), while others have argued for only modest changes (Tierney et al., 2019; O'Brien et al., 2014; Zhang et al., 2014). Steric (i.e., thermal) expansion of the oceans and substantially smaller polar ice sheets resulted in a global mean sea level approximately 20 m above modern (Dutton et al., 2015; Grant et al., 2019; Dumitru et al., 2019; Miller et al., 2020).

As global temperatures rise, global mean precipitation and the intensity of the heaviest precipitation events increase. As expressed in the Clausius-Clapeyron relation, saturation vapor pressure increases by approximately 7% K^{-1} of warming in the lower troposphere (Trenberth et al., 2003; Held and Soden, 2006). In a warmer world without major shifts in large-scale patterns of atmospheric circulation, column water vapor would continue to converge in areas already experiencing higher precipitation, while arid and semi-arid subtropical regions would become drier (Held and Soden, 2006; Seager et al., 2010; Trenberth, 2011). Thermodynamic constraints on the global-mean hydrologic cycle require a weakening of large-scale atmospheric circulation: as lower tropospheric water vapor increases, mass exchange between the boundary layer and mid-troposphere decreases, slowing the Hadley circulation (Held and Soden, 2006). Tropical precipitation dominates the global mean, so global water vapor residence time increases as convective mass fluxes slow, leading to a decrease in the ratio of precipitation to water vapor content (O'Gorman and Schneider, 2008). Overall, the impact of the elevated moisture content of warmer air is partially countered by constraints on mass fluxes in tropical convection, resulting in an increase in global-mean precipitation of approximately 2% K^{-1} of warming (Held and Soden, 2006).

Although it is challenging to place precise age constraints on terrestrial proxy reconstructions (Haywood et al., 2013a), paleobotanical data for the period from 3.6–2.6 Ma (mid to late Pliocene) reveal a generally wetter climate accompanied by a contraction of deserts and an expansion of forests, tropical savannas, and woodlands relative to the present (Salzmann et al., 2008). These data suggest wetter subtropical conditions and coincide with geological evidence of widespread lakes in presently dry regions, notably in subtropical Africa and western North America (Pound et al., 2014; Ibarra et al., 2018). Using a coupled climate model simulation with cloud albedo properties modified to reproduce early Pliocene sea surface temperature gradients, Burls and Fedorov (2017) argue that reduced meridional and zonal temperature gradients could have caused a reduction in subtropical moisture divergence sufficient to sustain subtropical wetting during the Pliocene, in contrast to future projections of near-term subtropical drying (Knutti and Sedláček, 2013). Thus, proxy reconstructions and modeling testify not only to an overall wetter climate, but also to dynamically-induced changes atmospheric circulation that would have altered regional patterns of precipitation.

We focus our attention on the extratropics, where water vapor is transported poleward primarily by atmospheric rivers (ARs; e.g., Zhu and Newell, 1994; Ralph et al., 2004; Newman et al., 2012; Payne et al., 2020). ARs are narrow plumes of water vapor transport typically associated with extratropical cyclones and breaking planetary waves, and draw their moisture from both tropical and subtropical sources (e.g., Bao et al., 2006; Knippertz and Wernli, 2010; Cordeira et al., 2013; Zhang et al., 2019). They bring large quantities of precipitation in fairly short periods of time, particularly when encountering topographic barriers (e.g., Ralph et al., 2006; Dettinger et al., 2011; Gimeno et al., 2014). Consequently, ARs play an important role in local weather and climate over land, contributing to local moisture budgets and causing the heavy rainfall events that lead to floods and landslides (Rutz et al., 2013). In the present-day, ARs account for up to half of the total annual precipitation along the west coasts of continents in extratropical latitudes (Dettinger et al., 2011; Viale et al., 2018). Understanding changes in the contribution of ARs to overall precipitation and their role in the most extreme precipitation events as the climate warms is therefore essential.

Similarly, planetary waves organize the location of storm tracks (Branstator, 1995; Chang et al., 2002; Son et al., 2009; Kaspi and Schneider, 2013; Tamarin and Kaspi, 2017), such that even small shifts can lead to strong impacts on regional climate (Neelin et al., 2013; Simpson et al., 2016; Shaw et al., 2016; Garfinkel et al., 2020). This is particularly true in the Northern Hemisphere, where stationary waves are most developed because of larger mountain ranges and more distinct land-ocean thermal contrasts. Certain robust responses of stationary waves to warming have been identified in models. These include, for example, a decrease in the stationary (i.e., resonant) wave number due to stronger mid-latitude westerlies (Simpson et al., 2016), and a weakening of winter (December–February) meridional winds (Vecchi and Soden, 2007; Haarsma and Selten, 2012; Wills and Schneider, 2018). Changes in stationary waves are a primary reason for departures from the "wet gets wetter, dry gets drier" response, which occurs when broad patterns of circulation remain approximately consistent (Held and Soden, 2006). With global warming, changes in the Northern Hemisphere stationary wave pattern will likely impact mid-latitude circulation and hydroclimate, but the precise nature of consequent changes in regional and hemispheric climate conditions remains elusive (Brandefelt and Körnich, 2008; Shepherd, 2014; Simpson et al., 2016).

2. Numerical experiments

We analyze a suite of simulations performed for PlioMIP2 with the University of Toronto version of the Community Climate System Model Version 4 (UofT-CCSM4) (Chandan and Peltier, 2017, 2018). UofT-CCSM4 is a coupled climate model with fully interacting atmosphere, ocean, land, and sea ice components, and has been modified from the original CCSM4 for the purposes of paleoclimate modeling (Chandan and Peltier, 2017). Specifically, the ocean model has been modified to remove the deep-water overflow parameterization that is related to the depths of sills in the present-day North Atlantic ocean (Danabasoglu et al., 2010), and the vertical profile of mixing has been modified by replacing the tidal mixing scheme—which is influenced by ocean bathymetry and coastlines, both of which were different during the Pliocene—with the simple depth-dependent profile of diapycnal diffusivity that was used in the ocean component (POP1) of the earlier CCSM3 model. The atmospheric component in CCSM4 is the Community Atmosphere Model version 4 (CAM4), which uses a finite volume grid with a nominal 1 degree horizontal resolution and 26 levels in the vertical. More detail about each component of the model can be found in Gent et al. (2011) and Chandan and Peltier (2017). Other versions of CCSM4, including the original model code, have been used in PlioMIP1 (Rosenbloom et al., 2013) and PlioMIP2 (Feng et al., 2020; Haywood et al., 2020).

The PlioMIP2 experiment protocol is based on the paleoenvironmental reconstructions of the Pliocene Research, Interpretation, and Synoptic Mapping Version 4 (PRISM4) dataset (Dowsett et al., 2016). To reduce uncertainty from temporal variability within the mid-Pliocene warm period (Salzmann et al., 2013), PRISM4 focuses on a time slice centered around the MIS KM5c interglacial peak at 3.205 Ma (Haywood et al., 2013a). Using the PRISM4 boundary conditions, UofT-CCSM4 simulates a mid-Pliocene climate that is in good agreement with a diverse array of proxies (Chandan and Peltier, 2017). The simulated mid-Pliocene climate is 3.8°C warmer than the pre-industrial, falling near the middle of estimates of mid-Pliocene warming simulated by PlioMIP2 models (Haywood et al., 2020). The UofT-CCSM4 PlioMIP2 simulation also exhibits increased seasonal temperature differences, including an amplification of average surface warming in the Northern

Hemisphere summer (Chandan and Peltier, 2017); this is not a robust feature across the ensemble of PlioMIP2 models (Haywood et al., 2020).

In Sections 3.1–3.3 we analyze 20 years of daily average and climatological mean data from simulations of the Pliocene, pre-industrial, and Modern-CO_2 climate experiments proposed by the PlioMIP2 experiment protocol (Haywood et al., 2016b). Differences between 20-year and 100-year climatological data from pre-industrial and Pliocene simulations are negligible compared to the differences between the simulations themselves (not shown); we are therefore confident that the changes discussed herein are driven by model boundary conditions rather than internal variability. The nomenclature that we use for these simulations, and other sensitivity simulations to be discussed later, follows the PlioMIP2 convention of labeling experiments as Ex^c, where x indicates boundary conditions different from the pre-industrial, and c is the CO_2 concentration in ppmv. Here x can be either "oi", "o", or "i", where "o" indicates modified orography (including PRISM4 land surface topography, bathymetry, rivers, lakes, and vegetation) and "i" designates Pliocene ice sheets (local albedo and topography); "oi" indicates both changes in combination. The mid-Pliocene simulation, Eoi^{400}, incorporates PRISM4 boundary conditions and sets pCO_2 to 400 ppmv. The pre-industrial control, E^{280}, uses boundary conditions appropriate for the pre-industrial and sets pCO_2 at 280 ppmv. The Modern-CO_2 simulation, E^{400}, uses the same boundary conditions as in the pre-industrial simulation save for pCO_2, which is set to 400 ppmv. In Section 3.4, we analyze several sensitivity simulations that toggle PRISM4 boundary conditions and CO_2 concentrations, and thereby allow us to identify the impacts of imposing and removing certain Pliocene boundary conditions. As in Chandan and Peltier (2018), we use 30 years of climatological data from these simulations, which are labeled Eoi^{280}, Eo^{400}, Eo^{280}, Ei^{400} and Ei^{280}, and are summarized in Table 1.

The PRISM4 paleogeography included in "o" boundary conditions is reconstructed by starting from modern-day topography (Amante and Eakins, 2009) and correcting it for the total influence of mantle convection (Moucha et al., 2008; Rowley et al., 2013) and the glacial isostatic response of the surface to the absence of Pliocene ice sheets (Dowsett et al., 2016). The most significant differences from the present-day (and from the previous PRISM reconstructions) are the closure of the Bering Strait and the Canadian Arctic Archipelago, and the infilling of the Hudson Bay. In "Eo" experiments, orography is not modified in areas where there are present-day ice sheets. Experiments with "o" boundary conditions impose terrestrial biomes from the reconstruction of Salzmann et al. (2008), and soils and lakes from the reconstruction of Pound et al. (2014).

Simulations with "i" boundary conditions include the PRISM4 ice sheets, which are reconstructed by combining Pliocene ice volume estimates from marine oxygen isotope records, bottom water temperature estimates, records of ice-rafted debris, and eustatic sea level estimates with land ice spatial extents from 3D thermo-mechanical ice-sheet models. The reconstruction includes the near-complete absence of the Greenland Ice Sheet and West Antarctic Ice Sheet, as well as a reduction in the volume of the East Antarctic Ice Sheet relative to present-day (Dowsett et al., 2016). The removal of modern ice sheets is accompanied by corresponding topographic and surface albedo changes.

Table 1
Summary of simulations from Chandan and Peltier (2017, 2018) employed in this study.

Experiment	Topography & Land*	Ice Sheets	CO_2 (ppmv)	Remarks
E^{280}	Modern	Modern	280	Pre-industrial control
E^{400}	Modern	Modern	400	Modern-CO_2 experiment, E^{400}-E^{280} isolates CO_2 forcing
Eoi^{400}	Pliocene	Pliocene	400	Pliocene experiment
Eoi^{280}	Pliocene	Pliocene	280	Eoi^{280}-E^{280} isolates orography and ice forcings
Eo^{280}	Pliocene	Modern	280	Eo^{280}-E^{280} isolates orography forcing
Eo^{400}	Pliocene	Modern	400	Eo^{400}-E^{280} isolates orography & CO_2 forcing
Ei^{280}	Modern	Pliocene	280	Ei^{280}-E^{280} isolates ice forcing
Ei^{400}	Modern	Pliocene	400	Ei^{400}-E^{280} isolates ice & CO_2 forcing

* Topography includes orography, bathymetry, land-sea mask, and river routing. Land includes vegetation, soils, and lakes.

Due to their interrelated nature, it is not entirely possible to cleanly isolate "o" and "i" boundary conditions. Over parts of West Antarctica, marine grounded ice sheets impact the land-sea mask. "Eo" simulations use a Pliocene land-sea mask in these areas, precluding a faithful representation of present-day ice sheets; "Ei" simulations replace these grounded marine ice sheets with very low topography. And to the extent that glacial isostatic adjustment from the lack of Pleistocene ice sheets is incorporated into PRISM4 paleogeography, the impacts of these ice sheets are also reflected in "o" boundary conditions. Chandan and Peltier (2017, 2018) provide further description of these simulations and their boundary conditions.

Finally, orbital parameters, trace gases, and aerosols are held constant in all simulations. Orbital forcing during the PRISM4 interval was similar to present-day (Haywood et al., 2013a), so all simulations use pre-industrial parameters, including a solar constant of 1365 Wm^{-2}, eccentricity 0.01624, obliquity 23.446°, and the longitude of perihelion 102.04°. CH_4, N_2O, CFCs, ozone, and aerosols are also held at pre-industrial values. Though the impacts of these trace gases and aerosols are minor compared to those of CO_2, the lack of proxies for their concentrations is a source of uncertainty (e.g., Hopcroft et al., 2020) in all simulations following the PlioMIP2 protocol.

3. Results

3.1. Global precipitation changes

Compared to the pre-industrial, global-mean surface temperature increases by 2°C in the Modern-CO_2 simulation and by 3.8°C in the Pliocene simulation. Global-mean precipitation increases by 0.11 mm day^{-1} in the Modern-CO_2 simulation and 0.22 mm day^{-1} in the Pliocene against a pre-industrial average of 2.91 mm day^{-1}. This corresponds to a roughly 2% increase in overall precipitation per K warming in both the Modern-CO_2 and Pliocene simulations. In both simulations, the "wet-gets-wetter" response is evident especially over the tropics, where increased moisture convergence strengthens the precipitation signature of the Intertropical Convergence Zone (ITCZ) (Fig. 1 a–b). Note that the appearance of a strong double ITCZ reflects a known shortcoming in the CCSM4 family of models (Gent et al., 2011). In the Pliocene simulation, some regional changes in precipitation can also be attributed to changes in topography. The higher elevations of the Andes, the Himalayas, and the Tibetan Plateau yield more abundant regional precipitation, and the exposed Sahul and Sunda shelves yield increased precipitation in Indonesia.

Extreme events are more sensitive to changes in variability than to changes in the mean (Katz and Brown, 1992), and both observations and models demonstrate higher variability in precipitation in warmer climates (Pendergrass et al., 2017; Rehfeld et al., 2020). As mean precipitation and precipitation variability increase, extreme precipitation events become more frequent and more intense. No single measure captures every relevant aspect of how precipitation extremes may change with warming (Donat et al., 2013; Schär et al., 2016; Pendergrass, 2018), in part because changes in frequency and intensity become more pronounced with the rareness of the event (Myhre et al., 2019). Here, we choose a metric that allows us to examine regional changes against the pre-industrial control: we define extreme precipitation as events exceeding the 99th percentile of daily pre-industrial precipitation in each grid point. Fig. 1 c–d shows the frequency of extreme

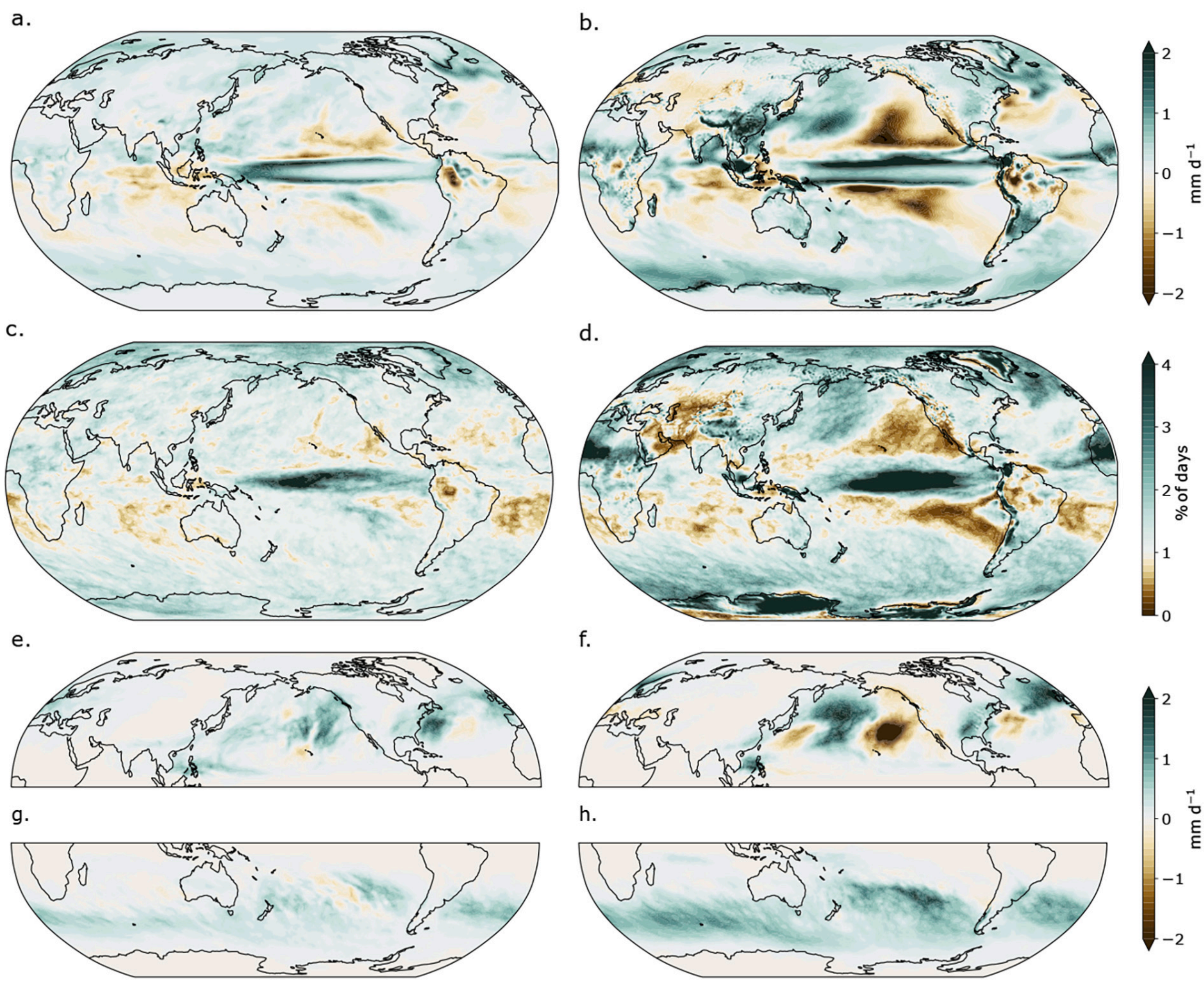

Fig. 1. Difference in annual mean precipitation, in mm day^{-1}, for the Modern-CO_2 minus pre-industrial (a) and Pliocene minus pre-industrial (b) simulations. Frequency of extreme precipitation, defined as daily precipitation exceeding the 99th percentile of pre-industrial control precipitation in each grid point (in % of days), for the Modern-CO_2 (c) and Pliocene (d) simulations. Difference in winter-time AR induced precipitation, in mm day^{-1}, for the Modern-CO_2 minus pre-industrial (e, g) and Pliocene minus pre-industrial (f, h). Winter-time is defined as December–February (DJF) in the Northern Hemisphere, and June–August (JJA) in the Southern Hemisphere. Figs. A1 and A2 depict corresponding pre-industrial values.

precipitation in the Modern-CO_2 and Pliocene simulations. Both simulations experience the largest increases in extreme precipitation in the tropics, where precipitation is largely determined by moist convection. In the extratropics, where extreme precipitation events scale neither with mean atmospheric water vapor content nor with mean moisture convergence at the base of storms (O'Gorman and Schneider, 2009), dynamic shifts in atmospheric circulation are of relatively greater consequence.

3.2. *Mid-latitude precipitation changes and the influence of atmospheric rivers*

The spatial pattern of change in extratropical extreme precipitation is especially heterogeneous in the Pliocene. Notably, pronounced changes take place over the east-central North Pacific, with distinct zonally asymmetric changes in both mean (Fig. 1 b) and extreme precipitation (Fig. 1 d). We turn our attention to processes affecting the extratropical hydrologic cycle in the North and South Pacific under Pliocene boundary conditions. In the warm season, modeled precipitation responses demonstrate an intensification of existing patterns in the hydrologic cycle, suggesting that such changes can be attributed in large part to the impacts of elevated CO_2. Therefore, we focus on moisture transport in the winter season—December–February (DJF) in the Northern Hemisphere, and June–August (JJA) in the Southern Hemisphere—when ARs are the most active.

To detect ARs, we use an algorithm that has previously been employed in paleoclimate studies (Lora et al., 2017; Skinner et al., 2020). We define ARs as contiguous regions of over 2000 km where vertically-integrated water vapor transport (IVT) exceeds a latitudinally-dependent threshold based on intergrated water vapor (IWV); that is,

$$IVT \geq IVT_{min}\left(1 - \frac{\overline{IWV}}{max\left(\overline{IWV}\right)}\right)^{-1},$$

where IVT_{min} is set equal to 225 kg m^{-1} s^{-1}, and $\overline{IWV}$ is the 30-day running average of zonal-mean IWV. This method allows for comparison between climates with different mean states, and is therefore well suited for the analysis presented herein. Fig. 1 e–f depicts winter-time AR precipitation, defined as daily precipitation coinciding with identified ARs.

Winter-time ARs differ substantially between the Modern-CO_2 and the Pliocene simulations, particularly over the North Pacific (Fig. 1 e–f). In the Modern-CO_2 simulation, AR precipitation increases over regions that already experience high AR activity in the pre-industrial simulation, highlighting the thermodynamic increase in overall precipitation in a warmer climate. Although the Pliocene simulation also produces more abundant AR precipitation in winter, there are stark spatial differences compared to the pre-industrial. This is especially evident over the North Pacific, where we observe a clear westward shift in AR activity accompanied by a decrease in AR precipitation over the central and eastern North Pacific.

To better understand the specific contribution of ARs to changes in total precipitation, we focus on two regions where ARs play a major role in the present climate. Specifically, we analyze precipitation along the coastal regions of North America and South America where ARs contribute substantially to water availability, snowpack variability, and the frequency and distribution of heavy precipitation (Ralph et al., 2006; Guan et al., 2010; Dettinger et al., 2011; Rutz and Steenburgh, 2012; Payne and Magnusdottir, 2014; Gimeno et al., 2016; Viale et al., 2018). These two regions of interest are indicated by red boxes in Fig. 2 a–b. We also identify AR extreme precipitation by the co-occurrence of extreme precipitation—again defined by the 99th percentile of the pre-industrial control at each grid point—and ARs.

Although the global and annual mean precipitation is 0.11 mm d^{-1} higher in the Pliocene simulation compared to the Modern-CO_2 simulation, the North American west coast is drier. Annually, the region defined from 32.5°N to 52.5°N and 230°E to 245°E (box in Fig. 2 a) receives 7% less precipitation and 13% less extreme precipitation than the Modern-CO_2 simulation, which we attribute to the waning influence of ARs. In the pre-industrial simulation, 27% of the total annual precipitation in this region of North America is attributable to ARs. While that share increases to 32% in the Modern-CO_2 simulation, it decreases to 22% in the Pliocene simulation. A similar but more drastic pattern of change occurs for extreme precipitation. Because of their tendency to produce short-lived, intense precipitation events, ARs account for as much as 75% of extreme precipitation in the pre-industrial simulation. That increases to 79% in the Modern-CO_2 simulation but decreases to 55% in the Pliocene.

Fig. 2 a shows the spatial relationship between changes in winter-time mean AR IVT and winter-time AR-induced extreme precipitation. In the Pliocene, the region influenced by ARs migrates westward, yielding more AR extreme precipitation over the west-central North Pacific and less AR extreme precipitation over the eastern North Pacific and the North American west coast. This is accompanied by changes in sea level pressure, which impact the trajectories of extratropical cyclones and accordingly the regions affected by ARs. Specifically, in the North Pacific, the position and intensity of the Aleutian Low pressure system exerts a substantial influence over North Pacific climate, and its strength is known to vary on sub-seasonal, inter-annual, and inter-decadal time-scales (Overland et al., 1999; Rodionov et al., 2007; Sugimoto and Hanawa, 2009). In the Pliocene simulation, the Aleutian Low is weakened, coinciding with anomalous anticyclonic flow compared to the pre-industrial simulation (Fig. 2 c). Consequently, IVT increases in the western and central North Pacific and decreases in the eastern North Pacific (Fig. 2 a). (In the Modern-CO_2 simulation, on the other hand, the Aleutian Low deepens slightly.)

In contrast to the Pacific coast of North America, the western coastal regions of South America see more abundant AR precipitation in the Pliocene. In the region defined from 38°S to 50°S and 280°E to 295°E (box in Fig. 2 b), overall precipitation varies little between the three simulations, while extreme precipitation increases monotonically from the pre-industrial to Modern-CO_2 to Pliocene simulation. ARs contribute 23% of total annual precipitation in the pre-industrial simulation, 27% in the Modern-CO_2 simulation, and 32% in the Pliocene. The fraction of extreme precipitation attributable to ARs remains 55% in each of the three simulations. In this region, the changes in zonal SLP anomalies and patterns of vapor transport are minor compared to the North Pacific. Atmospheric moisture content increases in response to warmer sea surface temperatures, enhancing the pre-industrial pattern of southwestward IVT and AR IVT. Changes in wintertime circulation, as demonstrated by the eddy streamfunction and wave activity flux (not shown), are negligible compared to the Northern Hemisphere.

The contrast between the North Pacific and the South Pacific precipitation and AR-induced precipitation responses highlights the interplay between the thermodynamic effects of warming and dynamic changes in moisture convergence. If circulation remains relatively similar to the pre-industrial, as in the South Pacific, ARs amplify existing patterns of precipitation. With more substantial changes in circulation, as in the North Pacific, AR changes may counter the thermodynamic

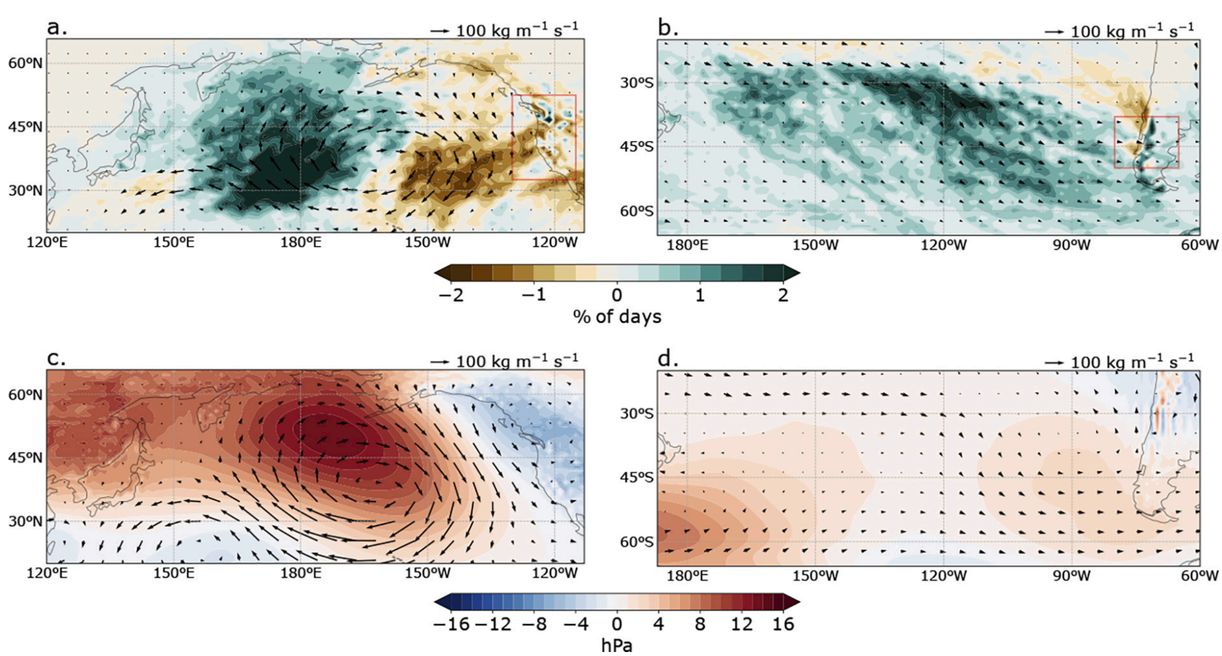

Fig. 2. (a, b) Shading of Pliocene minus pre-industrial changes in the frequency of AR extreme precipitation, defined as extreme precipitation events concomitant with ARs [% of days]. Vectors of changes in AR IVT [kg m^{-1} s^{-1}]. (c, d) Shading of Pliocene minus pre-industrial changes in sea level pressure anomalies [hPa], and vectors of changes in total IVT [kg m^{-1} s^{-1}]. (a and c) are for the Northern Hemisphere winter (DJF) season, while (b and d) are for the Southern Hemisphere winter (JJA) season. The North American and South American coastal regions referred to in the text are indicated on (a) and (b) with red boxes. Figs. A3 and A4 depict corresponding pre-industrial values.

effects of higher column water vapor in a warmer climate. These results also exemplify how thermodynamic factors influence different measures of precipitation (e.g., mean and extreme events) in different ways. ARs are important determinants of regional extreme precipitation, such that when ARs shift, extreme precipitation changes more drastically than mean precipitation.

3.3. Stationary wave response

We further explore these changes in the hydrologic cycle by studying changes in the zonally asymmetric circulation in relation to Northern Hemisphere wintertime stationary waves. To analyze stationary wave patterns we rely on the eddy streamfunction ψ^*, which is the zonally asymmetric component of the geostrophic streamfunction ψ. To represent stationary wave propagation, we calculate the wave activity flux described by (Plumb, 1985). The wave activity flux, which is nearly parallel to the group velocity and perpendicular to the phase lines of stationary waves, indicates the direction of stationary wave propagation.

In the pre-industrial simulation, a wave train emanates from East Asia and reflects back over the North Pacific, over North America, and back toward the tropical Atlantic (Fig. 3 a). In the Pliocene, this wave train is largely absent (Fig. 3 c). The streamfunction and Plumb flux differences in Fig. 3 e depict the waning of the pre-industrial stationary wave train. Signatures of stationary waves are evident on the Earth's surface in the form of anomalies in sea level pressure, and in the upper troposphere in the form of climatological wind fields. While the North Pacific mid-latitude jet stream is relatively strong and narrow in the pre-industrial climate (Fig. 3 b), it is weaker and spatially diffuse in the Pliocene simulation (Fig. 3 d). In Fig. 3 f, the weakening of zonal sea level pressure gradients corresponds with a weakening of the jet stream: shifts in the upper-troposphere westerly winds coincide with changes in zonal sea level pressure anomalies at the surface. Thus, the sea level pressure anomalies associated with regional changes in hydroclimate in Fig. 2 are tied to changes in the pattern of stationary wave propagation, as the diminishing of the pre-industrial Northern Hemisphere winter stationary wave train alters atmospheric circulation and teleconnection patterns in the Northern Hemisphere.

3.4. Sensitivity to Pliocene boundary conditions

We next analyze the sensitivity simulations to further assess the contributions of CO_2, topography, and ice sheets to changes in stationary waves and the corresponding shifts in extratropical circulation. Stationary waves are generated by zonal asymmetries in surface topography and diabatic heating (Valdes and Hoskins, 1989; Held et al., 2002). These forcings are interdependent: orographic features impact surface temperatures and diabatic heating (Nigam et al., 1986, 1988; Seager et al., 2002), while diabatic heating modifies the stationary wave response to orographic forcing (Ringler and Cook, 1999; Ting et al., 2001). Pliocene boundary conditions, therefore, cause changes in orography and surface temperatures that directly and indirectly affect the formation and propagation of stationary waves. Fig. 4 depicts the Pliocene minus pre-industrial differences in orography and DJF near-surface temperature: changes in elevation impact near-surface temperatures, as seen prominently over the Bering Strait and the Canadian

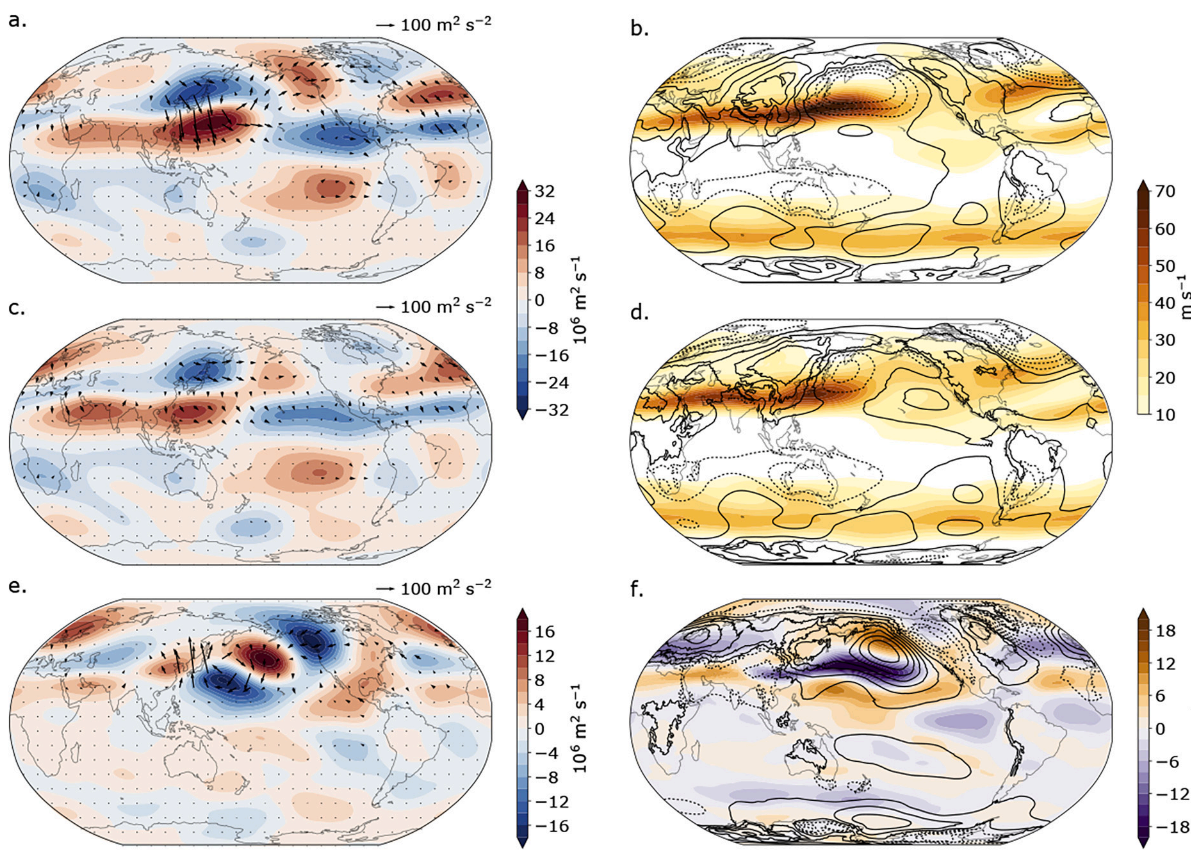

Fig. 3. 250 hPa eddy stream function (geostrophic stream function with the zonal mean removed; shading) and 250 hPa Plumb flux (vectors) for the pre-industrial (a), Pliocene (c), and Pliocene minus pre-industrial (e). 250 hPa zonal wind speeds (shading) and contours of zonal sea level pressure anomalies (zonal mean removed) for the pre-industrial (b), Pliocene (d), and Pliocene minus pre-industrial (f) simulations. Sea level pressure anomaly contours are show in 4 hPa intervals in plots d-e, and 2 hPa in the difference plot f, with solid lines representing positive values and dashed lines representing negative values. Zonal sea level pressure anomalies have been smoothed over continental regions for clarity. All panels show DJF climatologies.

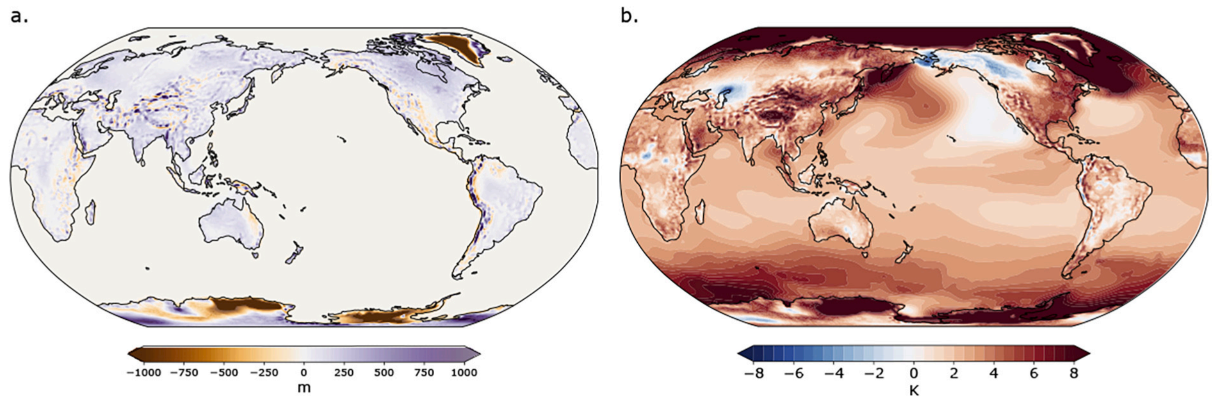

Fig. 4. Differences between Pliocene and pre-industrial simulations for surface elevation (a) and DJF reference height (2 m) temperature (b).

Archipelago (closed in Pliocene boundary conditions), as well as over Greenland and West Antarctica where extant ice sheets had not yet established.

We again use the DJF eddy streamfunction to diagnose changes in the stationary wave pattern. We find that while increasing CO_2 alone (Fig. 5 b) does not lead to appreciable changes in stationary waves, imposing "o" and "i" boundary conditions with constant CO_2 (Fig. 5 a) causes a response similar to the Pliocene minus pre-industrial case (Fig. 3 e). Furthermore, Fig. 5 c and 5 d demonstrate that the independent inclusion of Pliocene topography *or* Pliocene ice sheets causes a stationary wave response highly correlated with the circulation anomaly between the full Pliocene and pre-industrial simulations.

Corresponding sensitivity analyses for near-surface temperature reveal that imposing Pliocene topography and/or ice sheets results in cooling over the Northern Hemisphere continents and over the eastern North Pacific, with warming in most other parts of the world (Fig. 6 a, c, d). Chandan and Peltier (2017) noted similarities between the pattern of regional Northern Hemisphere cooling in the Pliocene winter and temperature trends in recent decades, which have been attributed to Arctic sea-ice loss causing an equatorward shift of the jet stream and intrusion of cold air over mid-latitude continents (Overland et al., 2011; Cohen et al., 2013, 2014). However, reanalysis data suggest that neither sea ice loss nor anthropogenic forcing causes this trend, and that the recent pattern is instead likely due to internal atmospheric variability (Sun et al., 2016; Blackport and Screen, 2020). If the latter interpretation is true, then these results demonstrate how Pliocene boundary conditions alter preferred patterns of atmospheric variability, leading to cooling in the mean wintertime near-surface temperature over Northern Hemisphere continents similar to the recent "Warm Arctic, Cold Continents" trend—while anthropogenic forcing alone (Fig. 6 b) yields amplified high-latitude warming without cooling over mid-latitude continents.

The DJF climatologies of reference height (2 m) temperature in Fig. 6 a,c, and d present a "horseshoe" pattern, with a cold temperature anomaly in the eastern North Pacific, resembling the negative ("cool") phase of the Pacific Decadal Oscillation (PDO) (Mantua et al., 1997; Mantua and Hare, 2002). In this phase, reduced cyclonic winds around a weakened Aleutian Low decrease northward advection of warm, moist air, resulting in stronger upwelling and cooler sea-surface temperatures along the coast of North America (Newman et al., 2016); coastal upwelling is responsible for the established relationship between weakened Aleutian Lows and California Current System cool events (Simpson, 1992; Fiedler and Mantua, 2017). But unlike the canonical PDO cool-phase pattern, cold sea surface temperature (SST) anomalies do not extend into the Eastern Tropical Pacific in Fig. 5 a, c, and d. This suggests that the PDO-like SST response owes its existence not to the atmospheric bridge (e.g., Alexander et al., 2002) or other teleconnections from the

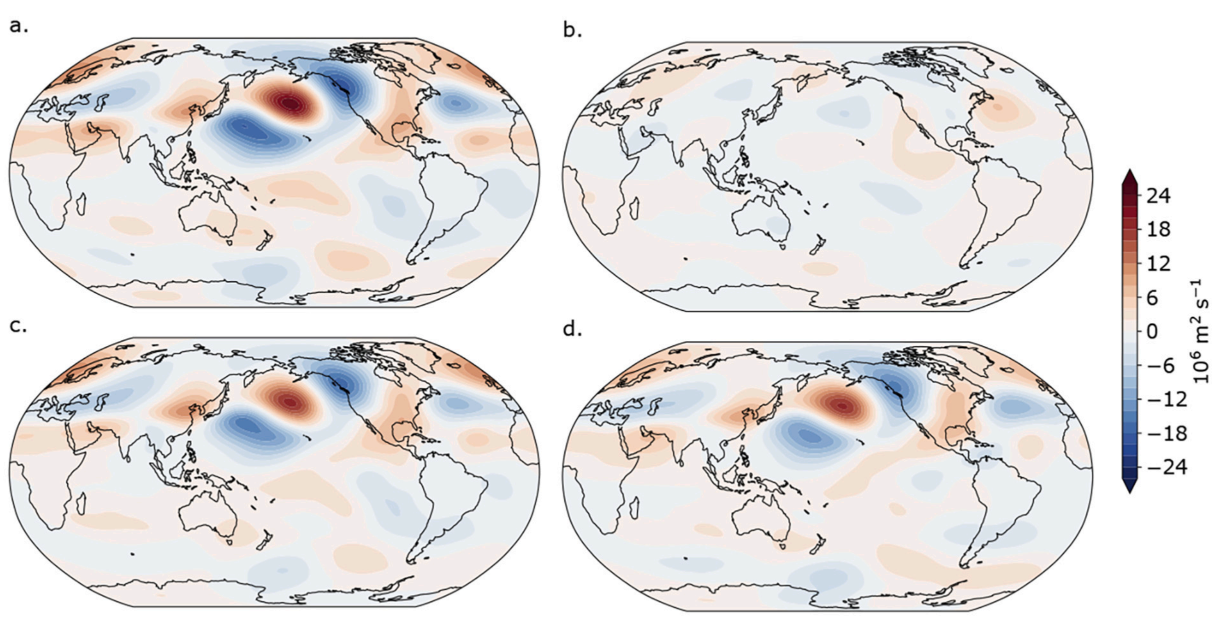

Fig. 5. Changes in the 250 hPa DJF climatological eddy streamfunction in our suite of sensitivity simulations. $Eoi^{400}-E^{400}$ (a), $E^{400}-E^{280}$ (b), $Eo^{400}-E^{400}$ (c), and $Ei^{400}-E^{400}$ (d).

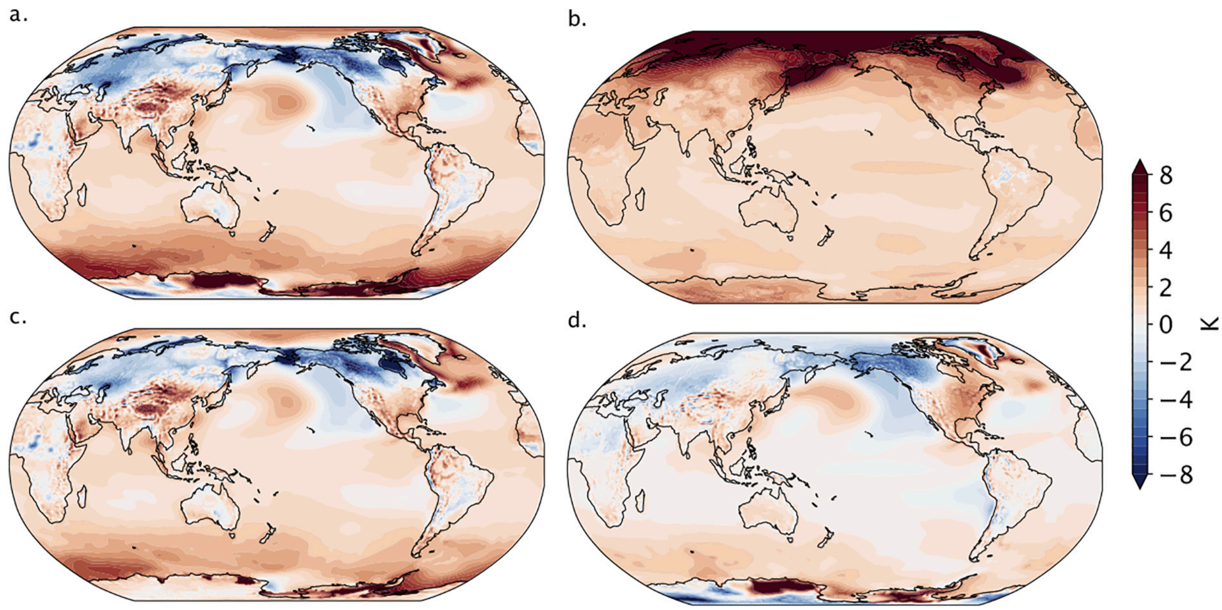

Fig. 6. Sensitivity tests for DJF reference height (2 m) temperature, in Kelvin. $Eoi^{400}-E^{400}$ (a), $E^{400}-E^{280}$ (b), $Eo^{400}-E^{400}$ (c), and $Ei^{400}-E^{400}$ (d).

tropical ocean, but to feedbacks originating from Pliocene surface boundary conditions.

Using intermediate-complexity idealized simulations, Garfinkel et al. (2020) demonstrated that Northern Hemisphere Winter stationary waves over the Pacific Ocean and North America respond non-additively to imposed forcings, with a ridge forming over the northeast Pacific and western North America only when land-sea contrasts, ocean horizontal heat transport, and topography are all imposed in combination. Our experiments, in which the pre-industrial Northern Hemisphere winter stationary wave pattern persists only in cases with neither Pliocene topography nor Pliocene ice-sheet forcing (Fig. 5), indicate similar nonlinear interactions at play. The *combination* of pre-industrial orography ice boundary conditions produces the distinct stationary wave pattern of Fig. 3a; consequently, when either set of boundary conditions is replaced with the Pliocene configuration, or when both are replaced, this stationary wave train diminishes. We leave a complete explication of these nonlinear stationary wave forcings to future work, but highlight here the influence of stationary waves on the hydrologic cycle: as is evident in Fig. 7, the Northern Hemisphere winter stationary wave response to Pliocene boundary conditions leaves a pronounced and zonally asymmetric signature on annual-mean precipitation over the Pacific and western North America.

4. Discussion

Pliocene land surface boundary conditions, which in some regions of the world were drastically different from modern, trigger nonlinear changes in planetary-scale teleconnection patterns that affect extratropical hydroclimate. These intricate interactions complicate efforts to apply the mid-Pliocene as a geologic process analog for understanding the impacts of ongoing greenhouse gas emission-driven warming. Past studies have invoked differences in tropical ocean feedbacks and the

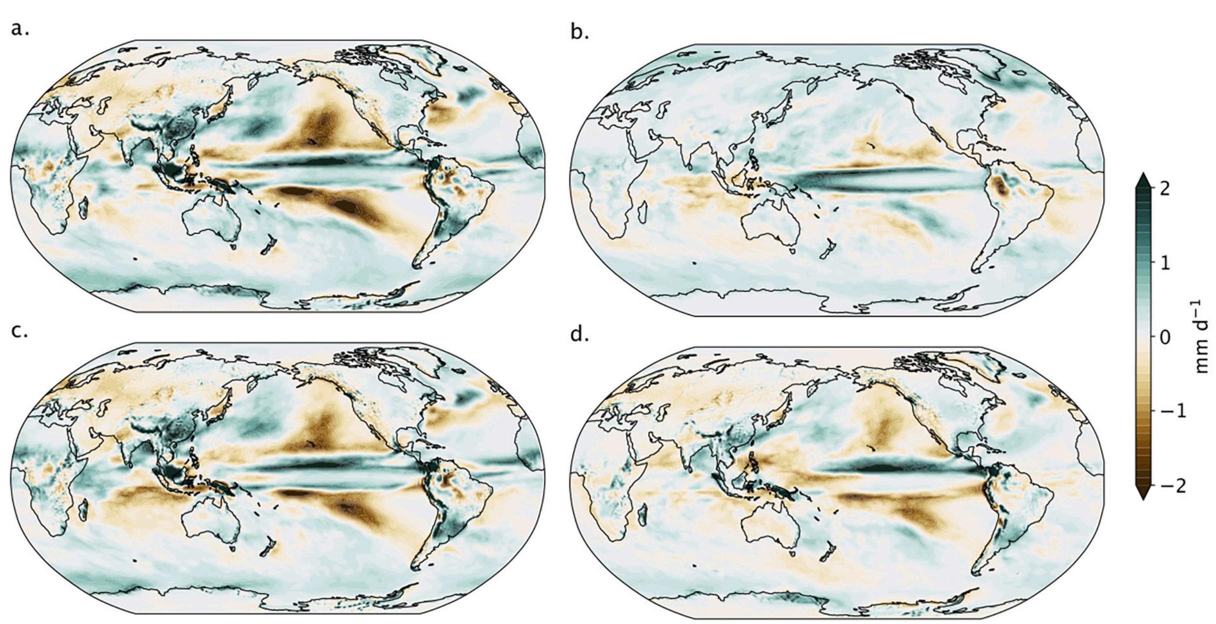

Fig. 7. Sensitivity tests for annual mean precipitation, in mm day^{-1}. $Eoi^{400}-E^{400}$ (a), $E^{400}-E^{280}$ (b), $Eo^{400}-E^{400}$ (c), and $Ei^{400}-E^{400}$ (d).

thermally driven Hadley circulation to explain features of mid-Pliocene hydroclimate (e.g., Fedorov et al., 2010; Goldner et al., 2011; Tierney et al., 2019), and to interpret proxy reconstructions (Burls and Fedorov, 2017; Ibarra et al., 2018). In the context of this existing body of literature, our results highlight the impact of high-latitude forcings, specifically changes in paleogeography and continental ice sheets, on extratropical precipitation patterns.

The dissimilar responses of regional hydrologic cycles along the Pacific coasts of North and South America demonstrate the impacts of competing physical processes, and illustrate the utility of studying ARs in the mid-Pliocene warm period. PlioMIP2 models largely agree on the direction of precipitation anomalies at high latitudes and in parts of the extratropics and subtropics (Haywood et al., 2020, Fig. A5). There is greater spread among models in swaths of the mid-latitudes, especially in the Northern Hemisphere (Haywood et al., 2020) where stationary waves are responsible for much of the spatial variability in precipitation (Wills and Schneider, 2016). A negative DJF precipitation anomaly in the eastern North Pacific, which resembles the AR precipitation shifts in Fig. 1 f, appears in some PlioMIP2 models and is evident in the multi-model mean (Fig. A5 b). Although not all PlioMIP2 modeling groups have published analyses of precipitation sensitivity to different boundary conditions, Chan and Abe-Ouchi (2020) reported, similar to our findings here, that the spatial patterns of precipitation in MIROC4m were more strongly affected by changes to Pliocene surface boundary conditions than by changes in atmospheric CO_2. Thus, attention to how boundary conditions affect ARs may help explain uncertainties in mid-latitude precipitation in the PlioMIP2 ensemble.

Studies of paleoclimate ARs focusing on the mid-Holocene (Skinner et al., 2020) and the Last Glacial Maximum (Lora et al., 2017; Lofverstrom, 2020) have shown that AR shifts likely caused changes to overall local precipitation that are evident in proxy records of the hydrologic cycle. Concerning the Pliocene, the western United States stands out due to the apparent model-data discrepancy it presents. In this area, proxy reconstructions of Pliocene hydroclimate suggest wetter-than-present conditions (Ibarra et al., 2018); on the other hand, our model and the PlioMIP2 multi-model mean show decreased precipitation (Haywood et al., 2020), a distinct change from PlioMIP1 (Haywood et al., 2013b). The Northern Hemisphere stationary wave response identified here is a possible mechanism by which PlioMIP2 boundary conditions may cause models to simulate decreased precipitation over the western United States.

Nevertheless, the limited spatial and temporal resolutions of hydrologic proxies make satisfactory model-data comparison difficult, and present a persistent obstacle to understanding mid-Pliocene warm period hydroclimate. PlioMIP2 focuses on a specific interglacial time-slice, which limits the availability of terrestrial proxy data relevant to model evaluation. Because even the relatively stable Pliocene climate would have varied on orbital time-scales (Salzmann et al., 2013; Haywood et al., 2013a), previous interpretations of hydroclimate proxies may not capture conditions during this narrowly defined time interval. As such, innovations in proxy reconstruction methods, closer analyses of published proxy data, water isotope-enabled model simulations, and further assessment of model sensitivity to orbital parameters would advance prospects for model-data comparison.

Moreover, because PlioMIP2 boundary conditions exert a strong influence on regional climate as demonstrated in this analysis, continued improvements to paleoenvironmental reconstructions of the mid-Pliocene will be essential. For example, while it has been established that Arctic ocean gateways substantially influence climate, their configuration during the mid-Pliocene warm period is still uncertain. Arctic gateways are closed in PlioMIP2 simulations, strengthening the Atlantic Meridional Overturning Circulation and allowing models to reproduce the enhanced high-latitude warming (Otto-Bliesner et al., 2017; Feng et al., 2017; Zhang et al., 2020) suggested by proxy records for sea surface temperature (Otto-Bliesner et al., 2017; Feng et al., 2017; Dowsett et al., 2019; Samakinwa et al., 2020). However, paleontological evidence and shoreline records indicate that the Bering Strait was open during parts of the Pliocene and early Pleistocene (Kaufman and Brigham-Grette, 1993; Goodfriend et al., 1996; Matthiessen et al., 2009). Reconstructing dynamic topography, glacial isostatic adjustment, and plate tectonics in this region will be crucial for understanding their impact on climate.

As a relatively accessible archive of how the Earth System responded to elevated warmth, the mid-Pliocene offers insight into changes that may emerge on the order of decades to centuries, depending on future greenhouse gas emissions (Burke et al., 2018). Researchers have used Pliocene simulations and reconstructions to make inferences about aspects of future climate change that are presently difficult to constrain, including regional mid-latitude hydroclimatic responses to warming. However, understanding whether particular characteristics of the mid-Pliocene are analogous to future conditions requires better knowledge of boundary conditions and their impact on climate. Our study demonstrates the importance of understanding paleoclimate ARs, exposing lines of inquiry that may improve our understanding of simulated Pliocene climates and their relevance, or lack thereof, to our own future.

5. Conclusions

In this study we analyze the UofT-CCSM4 simulations of Pliocene climate to gain insight into the hydrologic cycle of the mid-Pliocene warm period. While the overall precipitation increase is consistent with thermodynamic expectations, there are zonally asymmetric changes in mean and extreme precipitation in the extratropics, with pronounced regional impacts. These changes originate from wintertime differences in the behavior of atmospheric rivers, which in the North Pacific shift away from the west coast of North America. We attribute the changes in Northern Hemisphere precipitation and ARs to a stationary wave train that is present in the pre-industrial control simulation but largely absent in the mid-Pliocene simulation, corresponding with fewer ARs making landfall over western North America. A sensitivity analysis reveals that the shift in stationary waves is attributable to both the Pliocene topography and ice sheet forcings, which cause a nonlinear response in stationary waves regardless of CO_2 forcing. In mid-latitude regions where stationary waves and associated AR-driven precipitation are sensitive to surface boundary conditions, the mid-Pliocene warm period may not be an analog for the hydroclimatic impacts of anthropogenic warming.

Data availability

Data from the UofT-CCSM4 simulations are archived as monthly output in the PlioMIP2 data repository at the University of Leeds (Haywood et al., 2020). Additional data presented in this study are available from the authors upon request.

Author contributions

J.M.L. and S.M. designed the study. D.C. produced the numerical simulations. S.M. analyzed the data with contributions from all co-authors. S.M. wrote the manuscript with input from all co-authors.

Declaration of Competing Interest

The authors declare that they have no known competing financial interests or personal relationships that could have appeared to influence the work reported in this paper.

Acknowledgments

This study utilized high-performance computing resources from the Yale Center for Research Computing. To compute the streamfunction, we used the python package windspharm (Dawson, 2016). We thank the groups participating in PlioMIP2 for sharing their model output through the Earth System Grid Federation and PlioMIP2 database. We also thank two anonymous reviewers for their feedback, which helped improve this manuscript. M.L. is funded by the University of Arizona.

Appendix A. Supplementary data

Supplementary data to this article can be found online at https://doi.org/10.1016/j.gloplacha.2021.103557.

References

Alexander, M.A., Bladé, I., Newman, M., Lanzante, J.R., Lau, N.-C., Scott, J.D., 2002. The atmospheric bridge: the influence of ENSO teleconnections on Air–Sea interaction over the Global Oceans. J. Clim. 15 (16), 2205–2231.

Amante, C., Eakins, B.W., 2009. ETOPO1 1 Arc-Minute Global Relief Model. National Geophysical Data Center, NOAA.

Badger, M.P.S., Schmidt, D.N., Mackensen, A., Pancost, R.D., 2013. High-resolution alkenone palaeobarometry indicates relatively stable pCO2 during the Pliocene (3.3–2.8 Ma). Philos. Trans. R. Soc. A Math. Phys. Eng. Sci. 371, 20130094, 2001.

Bao, J.-W., Michelson, S.A., Neiman, P.J., Ralph, F.M., Wilczak, J.M., 2006. Interpretation of enhanced integrated water vapor bands associated with extratropical cyclones: their formation and connection to tropical moisture. Mon. Weather Rev. 134 (4), 1063–1080.

Bartoli, G., Hönisch, B., Zeebe, R.E., 2011. Atmospheric CO2 decline during the Pliocene intensification of Northern Hemisphere glaciations. Paleoceanography 26 (4).

Blackport, R., Screen, J.A., 2020. Weakened evidence for mid-latitude impacts of Arctic warming. Nat. Clim. Chang. 1–2.

Brandefelt, J., Körnich, H., 2008. Northern Hemisphere stationary waves in future climate projections. J. Clim. 21 (23), 6341–6353.

Branstator, G., 1995. Organization of storm track anomalies by recurring low-frequency circulation anomalies. J. Atmos. Sci. 52 (2), 207–226.

Burke, K.D., Williams, J.W., Chandler, M.A., Haywood, A.M., Lunt, D.J., Otto-Bliesner, B. L., 2018. Pliocene and Eocene provide best analogs for near-future climates. Proc. Natl. Acad. Sci. 115 (52), 13288–13293.

Burls, N.J., Fedorov, A.V., 2014. Simulating Pliocene warmth and a permanent El Niño-like state: the role of cloud albedo. Paleoceanography 29 (10), 893–910.

Burls, N.J., Fedorov, A.V., 2017. Wetter subtropics in a warmer world: contrasting past and future hydrological cycles. Proc. Natl. Acad. Sci. 114 (49), 12888–12893.

Chan, W.-L., Abe-Ouchi, A., 2020. Pliocene Model Intercomparison Project (PlioMIP2) simulations using the Model for Interdisciplinary Research on Climate (MIROC4m). Clim. Past 16 (4), 1523–1545.

Chandan, D., Peltier, W.R., 2017. Regional and global climate for the mid-Pliocene using the University of Toronto version of CCSM4 and PlioMIP2 boundary conditions. Clim. Past 13 (7), 919–942.

Chandan, D., Peltier, W.R., 2018. On the mechanisms of warming the mid-Pliocene and the inference of a hierarchy of climate sensitivities with relevance to the understanding of climate futures. Clim. Past 14 (6), 825–856.

Chang, E.K.M., Lee, S., Swanson, K.L., 2002. Storm track dynamics. J. Clim. 15 (16), 2163–2183.

Christina Ravelo, A., Simonne Dekens, P., McCarthy, M., 2006. Evidence for El Niño–like conditions during the Pliocene. GSA Today 16 (3), 4.

Cohen, J., Jones, J., Furtado, J.C., Tziperman, E., 2013. Warm Arctic, cold continents: a common pattern related to Arctic sea ice melt, snow advance, and extreme winter weather. Oceanography 26 (4), 150–160.

Cohen, J., Screen, J.A., Furtado, J.C., Barlow, M., Whittleston, D., Coumou, D., Francis, J., Dethloff, K., Entekhabi, D., Overland, J., Jones, J., 2014. Recent Arctic amplification and extreme mid-latitude weather. Nat. Geosci. 7 (9), 627–637.

Cordeira, J.M., Ralph, F.M., Moore, B.J., 2013. The development and evolution of two atmospheric rivers in proximity to Western North Pacific tropical cyclones in October 2010. Mon. Weather Rev. 141 (12), 4234–4255.

Danabasoglu, G., Large, W.G., Briegleb, B.P., 2010. Climate impacts of parameterized Nordic Sea overflows. J. Geophys. Res. Oceans 115 (C11).

Dawson, A., 2016. Windspharm: a high-level library for global wind field computations using spherical harmonics. J. Open Res. Software 4 (1), e31.

Dettinger, M.D., Ralph, F.M., Das, T., Neiman, P.J., Cayan, D.R., 2011. Atmospheric rivers, floods and the water resources of California. Water 3 (2), 445–478.

Donat, M.G., Alexander, L.V., Yang, H., Durre, I., Vose, R., Dunn, R.J.H., Willett, K.M., Aguilar, E., Brunet, M., Caesar, J., Hewitson, B., Jack, C., Tank, A.M.G.K., Kruger, A. C., Marengo, J., Peterson, T.C., Renom, M., Rojas, C.O., Rusticucci, M., Salinger, J., Elrayah, A.S., Sekele, S.S., Srivastava, A.K., Trewin, B., Villarroel, C., Vincent, L.A., Zhai, P., Zhang, X., Kitching, S., 2013. Updated analyses of temperature and precipitation extreme indices since the beginning of the twentieth century: the HadEX2 dataset. J. Geophys. Res. Atmos. 118 (5), 2098–2118.

Dowsett, H., Dolan, A., Rowley, D., Moucha, R., Forte, A.M., Mitrovica, J.X., Pound, M., Salzmann, U., Robinson, M., Chandler, M., Foley, K., Haywood, A., 2016. The PRISM4 (mid-Piacenzian) paleoenvironmental reconstruction. Clim. Past 12 (7), 1519–1538.

Dowsett, H.J., Robinson, M.M., Foley, K.M., Herbert, T.D., Otto-Bliesner, B.L., Spivey, W., 2019. The mid-Piacenzian of the North Atlantic Ocean. Stratigraphy 16 (3), 119–144.

Dumitru, O.A., Austermann, J., Polyak, V.J., Fornós, J.J., Asmerom, Y., Ginés, J., Ginés, A., Onac, B.P., 2019. Constraints on global mean sea level during Pliocene warmth. Nature 574 (7777), 233–236.

Dutton, A., Carlson, A.E., Long, A.J., Milne, G.A., Clark, P.U., DeConto, R., Horton, B.P., Rahmstorf, S., Raymo, M.E., 2015. Sea-level rise due to polar ice-sheet mass loss during past warm periods. Science 349 (6244).

Fedorov, A.V., Brierley, C.M., Emanuel, K., 2010. Tropical cyclones and permanent El Niño in the early Pliocene epoch. Nature 463 (7284), 1066–1070.

Fedorov, A.V., Burls, N.J., Lawrence, K.T., Peterson, L.C., 2015. Tightly linked zonal and meridional sea surface temperature gradients over the past five million years. Nat. Geosci. 8 (12), 975–980.

Feng, R., Otto-Bliesner, B.L., Fletcher, T.L., Tabor, C.R., Ballantyne, A.P., Brady, E.C., 2017. Amplified Late Pliocene terrestrial warmth in northern high latitudes from greater radiative forcing and closed Arctic Ocean gateways. Earth Planet. Sci. Lett. 466, 129–138.

Feng, R., Otto-Bliesner, B.L., Brady, E.C., Rosenbloom, N., 2020. Increased climate response and earth system sensitivity from CCSM4 to CESM2 in Mid-Pliocene simulations. J. Advan. Model. Earth Sys. 12 (8), e2019MS002033.

Fiedler, P.C., Mantua, N.J., 2017. How are warm and cool years in the California current related to ENSO? J. Geophys. Res. Oceans 122 (7), 5936–5951.

Garfinkel, C.I., White, I., Gerber, E.P., Jucker, M., Erez, M., 2020. The building blocks of Northern Hemisphere wintertime stationary waves. J. Clim. 33 (13), 5611–5633.

Gent, P.R., Danabasoglu, G., Donner, L.J., Holland, M.M., Hunke, E.C., Jayne, S.R., Lawrence, D.M., Neale, R.B., Rasch, P.J., Vertenstein, M., Worley, P.H., Yang, Z.-L., Zhang, M., 2011. The community climate system model Version 4. J. Clim. 24 (19), 4973–4991.

Gimeno, L., Nieto, R., Vázquez, M., Lavers, D.A., 2014. Atmospheric rivers: a mini-review. Front. Earth Sci. 2.

Gimeno, L., Dominguez, F., Nieto, R., Trigo, R., Drumond, A., Reason, C.J., Taschetto, A. S., Ramos, A.M., Kumar, R., Marengo, J., 2016. Major mechanisms of atmospheric moisture transport and their role in extreme precipitation events. Annu. Rev. Environ. Resour. 41 (1), 117–141.

Goldner, A., Huber, M., Diffenbaugh, N., Caballero, R., 2011. Implications of the Permanent El Niño teleconnection "Blueprint" for Past Global and North American Hydroclimatology. Clim. Past 7, 723–743.

Goodfriend, G.A., Brigham-Grette, J., Miller, G.H., 1996. Enhanced age resolution of the marine quaternary record in the Arctic using Aspartic acid Racemization dating of Bivalve Shells. Quat. Res. 45 (2), 176–187.

Grant, G.R., Naish, T.R., Dunbar, G.B., Stocchi, P., Kominz, M.A., Kamp, P.J.J., Tapia, C. A., McKay, R.M., Levy, R.H., Patterson, M.O., 2019. The amplitude and origin of sea-level variability during the Pliocene epoch. Nature 574, 237–241.

Guan, B., Molotch, N.P., Waliser, D.E., Fetzer, E.J., Neiman, P.J., 2010. Extreme snowfall events linked to atmospheric rivers and surface air temperature via satellite measurements. Geophys. Res. Lett. 37 (20).

Haarsma, R.J., Selten, F., 2012. Anthropogenic changes in the Walker circulation and their impact on the extra-tropical planetary wave structure in the Northern Hemisphere. Clim. Dyn. 39 (7), 1781–1799.

Haywood, A.M., Dolan, A.M., Pickering, S.J., Dowsett, H.J., McClymont, E.L., Prescott, C. L., Salzmann, U., Hill, D.J., Hunter, S.J., Lunt, D.J., Pope, J.O., Valdes, P.J., 2013a. On the identification of a Pliocene time slice for data–model comparison. Philos. Trans. R. Soc. A Math. Phys. Eng. Sci. 371 (2001):20120515.

Haywood, A.M., Hill, D.J., Dolan, A.M., Otto-Bliesner, B.L., Bragg, F., Chan, W.-L., Chandler, M.A., Contoux, C., Dowsett, H.J., Jost, A., Kamae, Y., Lohmann, G., Lunt, D.J., Abe-Ouchi, A., Pickering, S.J., Ramstein, G., Rosenbloom, N.A., Salzmann, U., Sohl, L., Stepanek, C., Ueda, H., Yan, Q., Zhang, Z., 2013b. Large-scale features of Pliocene climate: results from the Pliocene Model Intercomparison Project. Clim. Past 9 (1), 191–209.

Haywood, A.M., Dowsett, H.J., Dolan, A.M., 2016a. Integrating geological archives and climate models for the mid-Pliocene warm period. Nat. Commun. 7 (1).

Haywood, A.M., Dowsett, H.J., Dolan, A.M., Rowley, D., Abe-Ouchi, A., Otto-Bliesner, B., Chandler, M.A., Hunter, S.J., Lunt, D.J., Pound, M., Salzmann, U., 2016b. The Pliocene Model Intercomparison Project (PlioMIP) Phase 2: scientific objectives and experimental design. Clim. Past 12 (3), 663–675.

Haywood, A.M., Tindall, J.C., Dowsett, H.J., Dolan, A.M., Foley, K.M., Hunter, S.J., Hill, D.J., Chan, W.-L., Abe-Ouchi, A., Stepanek, C., Lohmann, G., Chandan, D., Peltier, W.R., Tan, N., Contoux, C., Ramstein, G., Li, X., Zhang, Z., Guo, C., Nisancioglu, K.H., Zhang, Q., Li, Q., Kamae, Y., Chandler, M.A., Sohl, L.E., Otto-Bliesner, B.L., Feng, R., Brady, E.C., von der Heydt, A.S., Baatsen, M.L.J., Lunt, D.J., 2020. The Pliocene model intercomparison project Phase 2: large-scale climate features and climate sensitivity. Clim. Past 16 (6), 2095–2123.

Held, I.M., Soden, B.J., 2006. Robust responses of the hydrological cycle to global warming. J. Clim. 19 (21), 5686–5699.

Held, I.M., Ting, M., Wang, H., 2002. Northern winter stationary waves: theory and modeling. J. Clim. 15 (16), 2125–2144.

Hopcroft, P.O., Ramstein, G., Pugh, T.A.M., Hunter, S.J., Murguia-Flores, F., Quiquet, A., Sun, Y., Tan, N., Valdes, P.J., 2020. Polar amplification of Pliocene climate by elevated trace gas radiative forcing. Proc. Natl. Acad. Sci. 117 (38), 23401–23407.

Ibarra, D.E., Oster, J.L., Winnick, M.J., Caves Rugenstein, J.K., Byrne, M.P., Chamberlain, C.P., 2018. Warm and cold wet states in the western United States during the Pliocene–Pleistocene. Geology 46 (4), 355–358.

Kageyama, M., Braconnot, P., Harrison, S.P., Haywood, A.M., Jungclaus, J.H., Otto-Bliesner, B.L., Peterschmitt, J.-Y., Abe-Ouchi, A., Albani, S., Bartlein, P.J., Brierley, C., Crucifix, M., Dolan, A., Fernandez-Donado, L., Fischer, H., Hopcroft, P. O., Ivanovic, R.F., Lambert, F., Lunt, D.J., Mahowald, N.M., Peltier, W.R., Phipps, S. J., Roche, D.M., Schmidt, G.A., Tarasov, L., Valdes, P.J., Zhang, Q., Zhou, T., 2018.

The PMIP4 contribution to CMIP6 – Part 1: overview and over-arching analysis plan. Geosci. Model Dev. 11 (3), 1033–1057.
Kaspi, Y., Schneider, T., 2013. The role of stationary eddies in shaping midlatitude storm tracks. J. Atmos. Sci. 70 (8), 2596–2613.
Katz, R.W., Brown, B.G., 1992. Extreme events in a changing climate: variability is more important than averages. Clim. Chang. 21 (3), 289–302.
Kaufman, D.S., Brigham-Grette, J., 1993. Aminostratigraphic correlations and paleotemperature implications, Pliocene-Pleistocene high-sea-level deposits, northwestern Alaska. Quat. Sci. Rev. 12 (1), 21–33.
Knippertz, P., Wernli, H., 2010. A lagrangian climatology of tropical moisture exports to the Northern Hemispheric Extratropics. J. Clim. 23 (4), 987–1003.
Knutti, R., Sedláček, J., 2013. Robustness and uncertainties in the new CMIP5 climate model projections. Nat. Clim. Chang. 3 (4), 369–373 (Number: 4 Publisher: Nature Publishing Group).
Lofverstrom, M., 2020. A dynamic link between high-intensity precipitation events in southwestern North America and Europe at the last Glacial Maximum. Earth Planet. Sci. Lett. 534, 116081.
Lora, J.M., Mitchell, J.L., Risi, C., Tripati, A.E., 2017. North Pacific atmospheric rivers and their influence on western North America at the Last Glacial Maximum. Geophys. Res. Lett. 44 (2), 1051–1059.
Mantua, N.J., Hare, S.R., 2002. The pacific decadal oscillation. J. Oceanogr. 58 (1), 35–44.
Mantua, N.J., Hare, S.R., Zhang, Y., Wallace, J.M., Francis, R.C., 1997. A pacific interdecadal climate oscillation with impacts on Salmon production. Bull. Am. Meteorol. Soc. 78 (6), 1069–1080.
Martínez-Botí, M.A., Foster, G.L., Chalk, T.B., Rohling, E.J., Sexton, P.F., Lunt, D.J., Pancost, R.D., Badger, M.P.S., Schmidt, D.N., 2015. Plio-Pleistocene climate sensitivity evaluated using high-resolution CO2 records. Nature 518 (7537), 49–54.
Matthiessen, J., Knies, J., Vogt, C., Stein, R., 2009. Pliocene palaeoceanography of the Arctic Ocean and subarctic seas. Philos. Trans. R. Soc. A Math. Phys. Eng. Sci. 367, 21–48, 1886.
McClymont, E.L., Ford, H.L., Ho, S.L., Tindall, J.C., Haywood, A.M., Alonso-Garcia, M., Bailey, I., Berke, M.A., Littler, K., Patterson, M.O., Petrick, B., Peterse, F., Ravelo, A. C., Risebrobakken, B., De Schepper, S., Swann, G.E.A., Thirumalai, K., Tierney, J.E., van der Weijst, C., White, S., Abe-Ouchi, A., Baatsen, M.L.J., Brady, E.C., Chan, W.-L., Chandan, D., Feng, R., Guo, C., von der Heydt, A.S., Hunter, S., Li, X., Lohmann, G., Nisancioglu, K.H., Otto-Bliesner, B.L., Peltier, W.R., Stepanek, C., Zhang, Z., 2020. Lessons from a high-CO_2 world: an ocean view from 3 million years ago. Clim. Past 16 (4), 1599–1615.
Miller, K.G., Browning, J.V., Schmelz, W.J., Kopp, R.E., Mountain, G.S., Wright, J.D., 2020. Cenozoic sea-level and cryospheric evolution from deep-sea geochemical and continental margin records. Sci. Adv. 6 (20), eaaz1346.
Moucha, R., Forte, A.M., Rowley, D.B., Mitrovica, J.X., Simmons, N.A., Grand, S.P., 2008. Mantle convection and the recent evolution of the Colorado Plateau and the Rio Grande Rift valley. Geology 36 (6), 439–442.
Myhre, G., Alterskjær, K., Stjern, C.W., Hodnebrog, Marelle, L., Samset, B.H., Sillmann, J., Schaller, N., Fischer, E., Schulz, M., Stohl, A., 2019. Frequency of extreme precipitation increases extensively with event rareness under global warming. Sci. Rep. 9 (1).
Neelin, J.D., Langenbrunner, B., Meyerson, J.E., Hall, A., Berg, N., 2013. California winter precipitation change under global warming in the coupled model intercomparison project Phase 5 ensemble. J. Clim. 26 (17), 6238–6256.
Newman, M., Kiladis, G.N., Weickmann, K.M., Ralph, F.M., Sardeshmukh, P.D., 2012. Relative contributions of synoptic and low-frequency eddies to time-mean atmospheric moisture transport, including the role of atmospheric rivers. J. Clim. 25 (21), 7341–7361.
Newman, M., Alexander, M.A., Ault, T.R., Cobb, K.M., Deser, C., Di Lorenzo, E., Mantua, N.J., Miller, A.J., Minobe, S., Nakamura, H., Schneider, N., Vimont, D.J., Phillips, A.S., Scott, J.D., Smith, C.A., 2016. The pacific decadal oscillation, revisited. J. Clim. 29 (12), 4399–4427.
Nigam, S., Held, I.M., Lyons, S.W., 1986. Linear simulation of the stationary eddies in a general circulation model. Part I: the no-mountain model. J. Atmos. Sci. 43 (23), 2944–2961.
Nigam, S., Held, I.M., Lyons, S.W., 1988. Linear simulation of the stationary eddies in a GCM. Part II: the "mountain" model. J. Atmos. Sci. 45 (9), 1433–1452.
de Nooijer, W., Zhang, Q., Li, Q., Zhang, Q., Li, X., Zhang, Z., Guo, C., Nisancioglu, K.H., Haywood, A.M., Tindall, J.C., Hunter, S.J., Dowsett, H.J., Stepanek, C., Lohmann, G., Otto-Bliesner, B.L., Feng, R., Sohl, L.E., Tan, N., Contoux, C., Ramstein, G., Baatsen, M.L.J., von der Heydt, A.S., Chandan, D., Peltier, W.R., Abe-Ouchi, A., Chan, W.-L., Kamae, Y., Brierley, C.M., 2020. Evaluation of Arctic warming in mid-Pliocene climate simulations. Clim. Past Discuss. 1–30.
O'Brien, C.L., Foster, G.L., Martínez-Botí, M.A., Abell, R., Rae, J.W.B., Pancost, R.D., 2014. High Sea surface temperatures in tropical warm pools during the Pliocene. Nat. Geosci. 7 (8), 606–611.
O'Gorman, P.A., Schneider, T., 2008. The hydrological cycle over a wide range of climates simulated with an idealized GCM. J. Clim. 21 (15), 3815–3832.
O'Gorman, P.A., Schneider, T., 2009. The physical basis for increases in precipitation extremes in simulations of 21st-century climate change. Proc. Natl. Acad. Sci. 106 (35), 14773–14777.
Otto-Bliesner, B.L., Jahn, A., Feng, R., Brady, E.C., Hu, A., Löfverström, M., 2017. Amplified North Atlantic warming in the late Pliocene by changes in Arctic gateways: Arctic Gateways and Pliocene climate. Geophys. Res. Lett. 44 (2), 957–964.
Overland, J.E., Adams, J.M., Bond, N.A., 1999. Decadal variability of the Aleutian Low and its relation to high-latitude circulation*. J. Clim. 12 (5), 1542–1548.
Overland, J.E., Wood, K.R., Wang, M., 2011. Warm Arctic—cold continents: climate impacts of the newly open Arctic Sea. Polar Res. 30 (1), 15787.
Pagani, M., Liu, Z., LaRiviere, J., Ravelo, A.C., 2010. High Earth-system climate sensitivity determined from Pliocene carbon dioxide concentrations. Nat. Geosci. 3 (1), 27–30.
Payne, A.E., Magnusdottir, G., 2014. Dynamics of Landfalling atmospheric rivers over the North Pacific in 30 years of MERRA reanalysis. J. Clim. 27 (18), 7133–7150.
Payne, A.E., Demory, M.-E., Leung, L.R., Ramos, A.M., Shields, C.A., Rutz, J.J., Siler, N., Villarini, G., Hall, A., Ralph, F.M., 2020. Responses and impacts of atmospheric rivers to climate change. Nature Rev. Earth Environ. 1 (3), 143–157.
Pendergrass, A.G., 2018. What precipitation is extreme? Science 360 (6393), 1072–1073 (Publisher: American Association for the Advancement of Science Section: Perspective).
Pendergrass, A.G., Knutti, R., Lehner, F., Deser, C., Sanderson, B.M., 2017. Precipitation variability increases in a warmer climate. Sci. Rep. 7 (1), 17966.
Plumb, R.A., 1985. On the three-dimensional propagation of stationary waves. J. Atmos. Sci. 42 (3), 217–229.
Pound, M., Tindall, J., Pickering, S., Haywood, A., Dowsett, H., Salzmann, U., 2014. Late Pliocene lakes and soils: a global data set for the analysis of climate feedbacks in a warmer world. Clim. Past 10 (1), 167–180.
Ralph, F.M., Neiman, P.J., Wick, G.A., 2004. Satellite and CALJET aircraft observations of atmospheric rivers over the Eastern North Pacific Ocean during the Winter of 1997/98. Mon. Weather Rev. 132 (7), 1721–1745.
Ralph, F.M., Neiman, P.J., Wick, G.A., Gutman, S.I., Dettinger, M.D., Cayan, D.R., White, A.B., 2006. Flooding on California's Russian River: role of atmospheric rivers. Geophys. Res. Lett. 33 (13).
Rehfeld, K., Hébert, R., Lora, J.M., Lofverstrom, M., Brierley, C.M., 2020. Variability of surface climate in simulations of past and future. Earth Sys. Dynam. 11 (2), 447–468.
Ringler, T.D., Cook, K.H., 1999. Understanding the seasonality of orographically forced stationary waves: interaction between mechanical and thermal forcing. J. Atmos. Sci. 56 (9), 1154–1174.
Rodionov, S.N., Bond, N.A., Overland, J.E., 2007. The Aleutian Low, storm tracks, and winter climate variability in the Bering Sea. Deep-Sea Res. II Top. Stud. Oceanogr. 54 (23), 2560–2577.
Rosenbloom, N.A., Otto-Bliesner, B.L., Brady, E.C., Lawrence, P.J., 2013. Simulating the mid-Pliocene warm period with the CCSM4 model. Geosci. Model Dev. 6 (2), 549–561.
Rowley, D.B., Forte, A.M., Moucha, R., Mitrovica, J.X., Simmons, N.A., Grand, S.P., 2013. Dynamic topography change of the Eastern United States since 3 million years ago. Science 340 (6140), 1560–1563.
Rutz, J.J., Steenburgh, W.J., 2012. Quantifying the role of atmospheric rivers in the interior western United States. Atmos. Sci. Lett. 13 (4), 257–261.
Rutz, J.J., Steenburgh, W.J., Ralph, F.M., 2013. Climatological characteristics of atmospheric rivers and their Inland Penetration over the Western United States. Mon. Weather Rev. 142 (2), 905–921.
Salzmann, U., Haywood, A.M., Lunt, D.J., Valdes, P.J., Hill, D.J., 2008. A new global biome reconstruction and data-model comparison for the Middle Pliocene. Glob. Ecol. Biogeogr. 17 (3), 432–447.
Salzmann, U., Dolan, A.M., Haywood, A.M., Chan, W.-L., Voss, J., Hill, D.J., Abe-Ouchi, A., Otto-Bliesner, B., Bragg, F.J., Chandler, M.A., Contoux, C., Dowsett, H.J., Jost, A., Kamae, Y., Lohmann, G., Lunt, D.J., Pickering, S.J., Pound, M.J., Ramstein, G., Rosenbloom, N.A., Sohl, L., Stepanek, C., Ueda, H., Zhang, Z., 2013. Challenges in quantifying Pliocene terrestrial warming revealed by data–model discord. Nat. Clim. Chang. 3 (11), 969–974.
Samakinwa, E., Stepanek, C., Lohmann, G., 2020. Sensitivity of mid-Pliocene climate to changes in orbital forcing and PlioMIP's boundary conditions. Clim. Past 16 (4), 1643–1665.
Schär, C., Ban, N., Fischer, E.M., Rajczak, J., Schmidli, J., Frei, C., Giorgi, F., Karl, T.R., Kendon, E.J., Tank, A.M.G.K., O'Gorman, P.A., Sillmann, J., Zhang, X., Zwiers, F.W., 2016. Percentile indices for assessing changes in heavy precipitation events. Clim. Chang. 137 (1), 201–216.
Seager, R., Battisti, D.S., Yin, J., Gordon, N., Naik, N., Clement, A.C., Cane, M.A., 2002. Is the Gulf Stream responsible for Europe's mild winters? Q. J. R. Meteorol. Soc. 128 (586), 2563–2586.
Seager, R., Naik, N., Vecchi, G.A., 2010. Thermodynamic and dynamic mechanisms for large-scale changes in the Hydrological Cycle in response to global warming. J. Clim. 23 (17), 4651–4668.
Shaw, T.A., Baldwin, M., Barnes, E.A., Caballero, R., Garfinkel, C.I., Hwang, Y.-T., Li, C., O'Gorman, P.A., Rivière, G., Simpson, I.R., Voigt, A., 2016. Storm track processes and the opposing influences of climate change. Nat. Geosci. 9 (9), 656–664.
Shepherd, T.G., 2014. Atmospheric circulation as a source of uncertainty in climate change projections. Nat. Geosci. 7 (10), 703–708.
Simpson, I.R., Seager, R., Ting, M., Shaw, T.A., 2016. Causes of change in Northern Hemisphere winter meridional winds and regional hydroclimate. Nat. Clim. Chang. 6 (1), 65–70.
Simpson, J.J., 1992. Response of the Southern California current system to the mid-latitude North Pacific coastal warming events of 1982–1983 and 1940–1941. Fish. Oceanogr. 1 (1), 57–79.
Skinner, C.B., Lora, J.M., Payne, A.E., Poulsen, C.J., 2020. Atmospheric river changes shaped mid-latitude hydroclimate since the mid-Holocene. Earth Planet. Sci. Lett. 541, 116293.
Son, S.-W., Ting, M., Polvani, L.M., 2009. The effect of topography on storm-track intensity in a relatively simple general circulation model. J. Atmos. Sci. 66 (2), 393–411.

Sugimoto, S., Hanawa, K., 2009. Decadal and interdecadal variations of the Aleutian Low activity and their relation to Upper Oceanic Variations over the North Pacific. J. Meteorol. Soc. Jpn. Ser. II 87 (4), 601–614.
Sun, L., Perlwitz, J., Hoerling, M., 2016. What caused the recent "Warm Arctic, Cold Continents" trend pattern in winter temperatures? Geophys. Res. Lett. 43 (10), 5345–5352.
Tamarin, T., Kaspi, Y., 2017. Mechanisms controlling the downstream poleward deflection of midlatitude storm tracks. J. Atmos. Sci. 74 (2), 553–572.
Tierney, J.E., Haywood, A.M., Feng, R., Bhattacharya, T., Otto-Bliesner, B.L., 2019. Pliocene warmth consistent with greenhouse gas forcing. Geophys. Res. Lett. 46 (15), 9136–9144.
Ting, M., Wang, H., Yu, L., 2001. Nonlinear stationary wave maintenance and seasonal cycle in the GFDL R30 GCM. J. Atmos. Sci. 58 (16), 2331–2354.
Trenberth, K., 2011. Changes in precipitation with climate change. Clim. Res. 47 (1), 123–138.
Trenberth, K.E., Dai, A., Rasmussen, R.M., Parsons, D.B., 2003. The changing character of precipitation. Bull. Am. Meteorol. Soc. 84 (9), 1205–1218.
Valdes, P.J., Hoskins, B.J., 1989. Linear stationary wave simulations of the time-mean climatological flow. J. Atmos. Sci. 46 (16), 2509–2527.
Vecchi, G.A., Soden, B.J., 2007. Global warming and the weakening of the tropical circulation. J. Clim. 20 (17), 4316–4340.
Viale, M., Valenzuela, R., Garreaud, R.D., Ralph, F.M., 2018. Impacts of atmospheric rivers on precipitation in Southern South America. J. Hydrometeorol. 19 (10), 1671–1687.
Wara, M.W., Ravelo, A.C., Delaney, M.L., 2005. Permanent El Nino-like Conditions during the Pliocene warm period. Science 309 (5735), 758–761.
Wills, R.C., Schneider, T., 2016. How stationary eddies shape changes in the hydrological cycle: zonally asymmetric experiments in an idealized GCM. J. Clim. 29 (9), 3161–3179.
Wills, R.C.J., Schneider, T., 2018. Mechanisms setting the strength of orographic rossby waves across a wide range of climates in a moist idealized GCM. J. Clim. 31 (18), 7679–7700.
Zhang, Y.G., Pagani, M., Liu, Z., 2014. A 12-million-year temperature history of the tropical pacific ocean. Science 344 (6179), 84–87.
Zhang, Z., Ralph, F.M., Zheng, M., 2019. The relationship between extratropical cyclone strength and atmospheric river intensity and position. Geophys. Res. Lett. 46 (3), 1814–1823.
Zhang, Z., Li, X., Guo, C., Otterå, O.H., Nisancioglu, K.H., Tan, N., Contoux, C., Ramstein, G., Feng, R., Otto-Bliesner, B.L., Brady, E., Chandan, D., Peltier, W.R., Baatsen, M.L.J., von der Heydt, A.S., Weiffenbach, J.E., Stepanek, C., Lohmann, G., Zhang, Q., Li, Q., Chandler, M.A., Sohl, L.E., Haywood, A.M., Hunter, S.J., Tindall, J. C., Williams, C., Lunt, D.J., Chan, W.-L., Abe-Ouchi, A., 2020. Mid-Pliocene Atlantic Meridional Overturning Circulation simulated in PlioMIP2. Clim. Past Discuss. 1–22.
Zhu, Y., Newell, R.E., 1994. Atmospheric rivers and bombs. Geophys. Res. Lett. 21 (18), 1999–2002.